Chapter 6 Image Fusion

The PCNN is a biologically inspired neural network, widely applied in the field of image processing such as the image segmentation, image enhancement, and pattern recognition. This chapter will describe its application in image fusion. Firstly, it will briefly review the development of the image fusion based on the PCNN, and then simply introduce some medical image fusion methods [1]. Finally, it will describe a new method of the multi-focus image fusion suggested in Ref. [2].

6.1 PCNN and Image Fusion

First of all, the foundation of the image fusion, including its definition, hierarchical division and application fields, is briefly reviewed. And then the development of the PCNN in the field of the image fusion is explained.

6.1.1 Preliminary of Image Fusion

The image fusion is an important branch of data fusion that refers to the process of combining data from different sources together so that the fused data provide the most detailed and reliable information as far as possible. Therefore, the image fusion is usually defined as the process of combining relevant information from two or more images into a single image, also known as the fused image. Undoubtedly, the fused image will be more informative than any of the input images [3].

Therefore, the fused image has many advantages: (a) It contains more complete and accurate information; (b) It has higher reliability and robustness; (c) It is easier to be understood by user and computer.

Y. Ma et al., *Applications of Pulse-Coupled Neural Networks*

The image fusion is generally divided into three levels: pixel-level fusion, feature-level fusion, and decision-level fusion. The difference of these three levels is that they have different objects of study. Pixel-level fusion belongs to low-level fusion which is the foundation of the others. Pixel-level fusion directly computes the final value of every pixel from input images based on some rules.

Until now the image fusion technique has been widely applied into many fields such as the defense industry, robot vision, digital camera application (e.g., multi-focus image fusion), medical imaging, and satellite image(e.g., remote sensing image).

6.1.2 Applications in Image Fusion

Speaking of the image fusion method, people tend to think of wavelet or pyramid algorithm [4 – 11], because these methods are usually used to fuse object images. However, the PCNN has a potential ability of the image fusion in its own way. For instance, as early as 1998, Kinser had used this ability to study the spiral image fusion [12]. He proposed the PCNN-based spiral image fusion system and employed inter-channel autowave communication to combine the information from the different channels.

Subsequently, many approaches about the image fusion based on the PCNN have been published in different journals or proceedings. Generally, these PCNN-based algorithms can be divided into two groups.

One is to fuse images together with other methods (e.g., wavelet theory). For example, Broussard et al., firstly segmented the image with the PCNN and then the segmented feature objects and the original image were fused to improve the rate of object recognition [13]. Blasch segmented image, extracted and linked spatial features based on the PCNN, then fused current and learned information with the belied filter [14]. Xu and Chen decomposed the image via the multi-scale contrast pyramid, and subsequently utilized the global coupling property and the synchronous pulse burst property of the PCNN to select the best contrast component from original images [15]. Similarly, Li and Zhu used wavelet packet to decompose the original images into a series of frequency components, and then employed the PCNN to make the decision for choice of fusing frequency components [16]. The other is to only

use the PCNN to finish the whole task of the image fusion. Zhang and Liang designed a parallel image fusion system only using a master PCNN and some assistant PCNNs [17]. Li and Tan proposed a region-based image fusion of the PCNN [18]. Firstly, the input image was segmented into different regions, and then the fusion weight coefficient was determined according to the values of salience [18] and visibility [18] of each region, reflecting its clarity. The above schemes have a common trait: they have to run more than one PCNN in parallel. Different from them, Wang and Ma presented a method of image fusion with a single modified PCNN and applied it into medical image fusion [1, 2]. For multi-focus image fusion, Miao and Wang designed an adaptive image fusion algorithm via automatic change of the linking coefficient [19]. Huang and Jing decomposed source image into blocks and reconstructed the final fused image by selecting the image blocks from the source images based on the comparison of the outputs of the PCNN [20].

6.2 Medical Image Fusion

Medical image fusion not only is useful in diagnosing diseases, but also reduces the storage cost by a single fused image instead of multiple source images. Many approaches, such as FSD pyramid [4], gradient pyramid [5], Laplacian pyramid [6], DWT pyramid [7], SIDWT pyramid [8], morphological pyramid [9], ratio pyramid [10], and contrast pyramid [11], have been proposed. Until now, there is not any general method suitable for all kinds of applications, each method is only efficient for specific types of images and each has its own limits. For example, the contrast pyramid method loses too much information in the source images during the process of fusion; the ratio pyramid method produces lots of false information that does not exist in the source images; and morphological pyramid method creates many bad edges. In a word, these methods cannot deal with various types of medical images. In this chapter, another method of the medical image fusion based on a modified model of the PCNN, that is, the multiple-image fusion with the m-PCNN, is described in detail.

6.2.1 Description of Model

In fact, only one stimulus for each neuron is an obstacle for the multiple-image fusion with the basic PCNN. Here, a new fusion method, which is based on the m-PCNN model, is suggested and its expressions have been described in Chapter 1, as shown in Fig. 6.1. Like the original PCNN neuron, each m-PCNN neuron also consists of three parts: dendritic tree, information fusion, and pulse generator. The role of the dendritic tree is to receive two kinds of inputs. The one is from the external stimulus and the other is from the surrounding neurons. The task of the information fusion part is to fuse all data from dendrite tree part. The role of the pulse generator is to generate the output pulse.

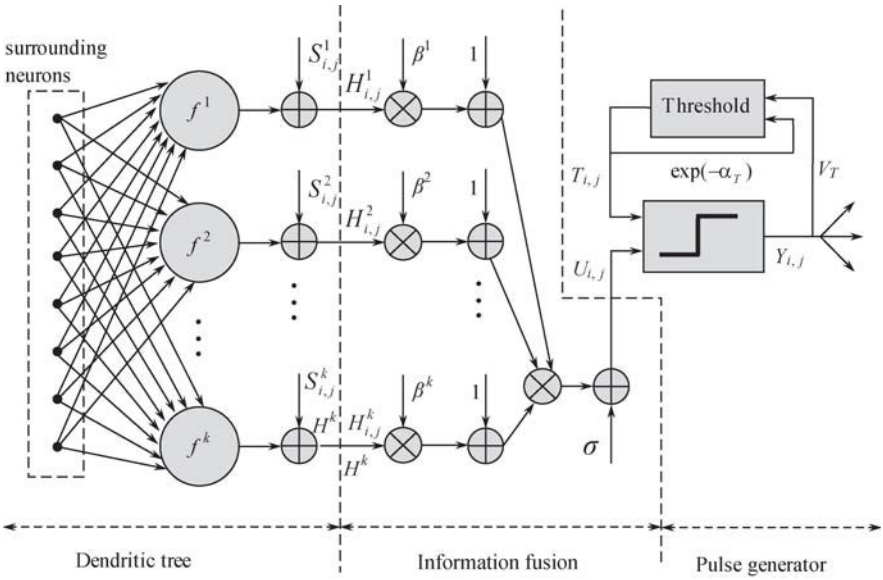

Fig. 6.1. The neuromime of the m-PCNN

When used in the image fusion, the m-PCNN is a single layer two-dimensional array of laterally linked neurons and all neurons are identical. The number of neurons in the network is equal to the number of pixels in each input image. The gray value of a pixel is taken as the stimulus of the neuron. For the same neuron, its stimuli come from the gray value of its corresponding pixels in different images, which have the same position. The

data fusion is finished in the interior activation of the neuron by means of internal activity. Note that external input images must be registered and all inputs should also have the identical resolution.

Using one m-PCNN can fuse multiple-source images. Multiple external stimuli work in a neuron at the same time, which makes multiple images processed in a parallel way and less time-consuming in the process of image fusion and cuts down computational complexity as well.

6.2.2 Image Fusion Algorithm

The m-PCNN makes the process of image fusion very simple and efficient. The algorithm is implemented via Fig. 6.2 and described in detail as follows:

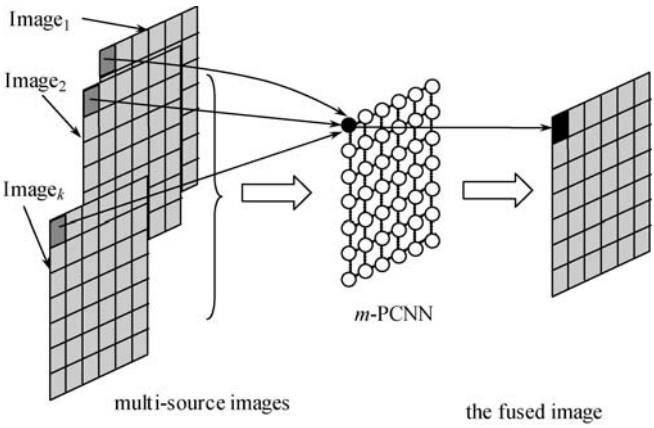

Fig. 6.2. The scheme of the m-PCNN image fusion algorithm

(1) Multi-source images are taken as multiple stimuli of the m-PCNN. Let I^k denotes multi-source images, generally $k > 1$. Namely, $S^k = I^k$. Note that all external input images must be registered and also have the same size and identical resolution.

(2) The stimuli and feed information are transmitted into the neuron via their different channels.

(3) All received signals are mixed together in the internal activity of the neuron. From Eq. (1.27), there are not only linear operations but also nonlinear operations in the process of data fusion.

(4) The pulse generator determines the firing events according to the

current threshold. The parameter C_n is used to record the number of the fired neurons at the current iteration. Note that each neuron only fires once in the whole process.

(5) Make $Sum = Sum' + C_n$, where Sum denotes the total number of the fired neurons after the current iteration. $Sum\prime$ denotes the total number of the fired neurons before the current iteration.

(6) If $Sum < Num$, turn to (2); otherwise, continue. Num means the total number of all neurons in the network.

(7) Normalize the internal state U. The normalized U is the fused image.

Because data fusion happens in the internal activity, the internal state U includes all information needed by fusion. But U could not be directly taken as the final output image, because some values of U may be beyond the value of the dynamic range of the image, it is necessary to adjust U by the linear transformation.

6.2.3 Experimental Results and Analysis

In the experiments, the m-PCNN is taken to fuse different medical images, and its parameters are set empirically as follows:

Table 6.1. Parameters of the m-PCNN in the experiment.

parameters	m	β^1	β^2	σ	α_T	V_T
value	2	0.5	0.5	1.0	0.012	4000

Its convolution core

$$K = \begin{bmatrix} 0.1091, & 0.1409, & 0.1091 \\ 0.1409, & 0, & 0.1409 \\ 0.1091, & 0.1409, & 0.1091 \end{bmatrix}$$

and $M(\cdot) = W(\cdot) = Y[n-1] \otimes K$, where $\otimes$ denotes convolution operation.

As shown in Figs. 6.3 – 6.6, corresponding to groups 1 – 4, the first two images are used as the experiment images. Figs. 6.3(a) and (b) come from internet [21], Figs. 6.4(a) and (b) come from Ref. [22]. Figs. 6.5(a) and (b), Figs. 6.6(a) and (b) the come from the website of the Atlas project (which is made possible in part by the Departments of Radiology and Neurology at Brigham and Women's Hospital), Harvard Medical School, the Countway Library of Medicine, and the American Academy of Neurology [23].

In order to evaluate the performance of the algorithm, it is compared with other methods: contrast pyramid, FSD pyramid, gradient pyramid, Laplacian pyramid, morphological pyramid, ratio pyramid, SIDWT with Harr, and DWT with DBSS (2, 2). In the experimental images for groups 1 – 2, Figs. 6.3(a) and (b) and Figs. 6.4(a) and (b) are source images. Figs. 6.3(c) and 6.4(c) are the fused images, the output of the m-PCNN algorithm.

The subsequent images, Figs. 6.3(d) – (i) and Figs. 6.4(d) – (i), are fused by various pyramid algorithms.

The next images, Figs. 6.3(j), (k) and Figs. 6.4(j), (k) are mixed by wavelet transform. Image (j) is obtained by the approach of shift invariant discrete wave transform (SIDWT) with Harr. Image (k) is fused by discrete wavelet transform (DWT), and wavelet is the DBSS (2, 2).

Parameters of these two methods are set by:

pyramid level = 4,

selection rules: highpass = max,

lowpass = average.

The last two images, Figs. 6.3(l) and 6.4(l) are obtained by calculating the average of source images.

In fact, the image fusion is to fuse a variety of multi-source images together and creates a fused image that acquires as much information from each of the source images as possible. The more information obtained from source images, the better the effect of fusion is. The mutual information is used as the objective standard to estimate the performance of different methods included here. It can measure the similarity between two original images. If these two images are more similar, the value of mutual information is larger. Therefore, mutual information will be able to measure the performance of different methods.

In Figs. (6.7) – (6.10), MI_AF denotes mutual information between image A and the fused image F; it is calculated according to Eq. (6.1).

$$\text{MI\_AF} = H(A) + H(F) - H(A, F), \tag{6.1}$$

where $H(A, F)$ is joint entropy,

$$H(A, F) = -\sum p(A, F) \log p(A, F), \tag{6.2}$$

MI_BF denotes the mutual information between image B and the fused image F; MI_AB denotes the cumulative mutual information which is the sum of

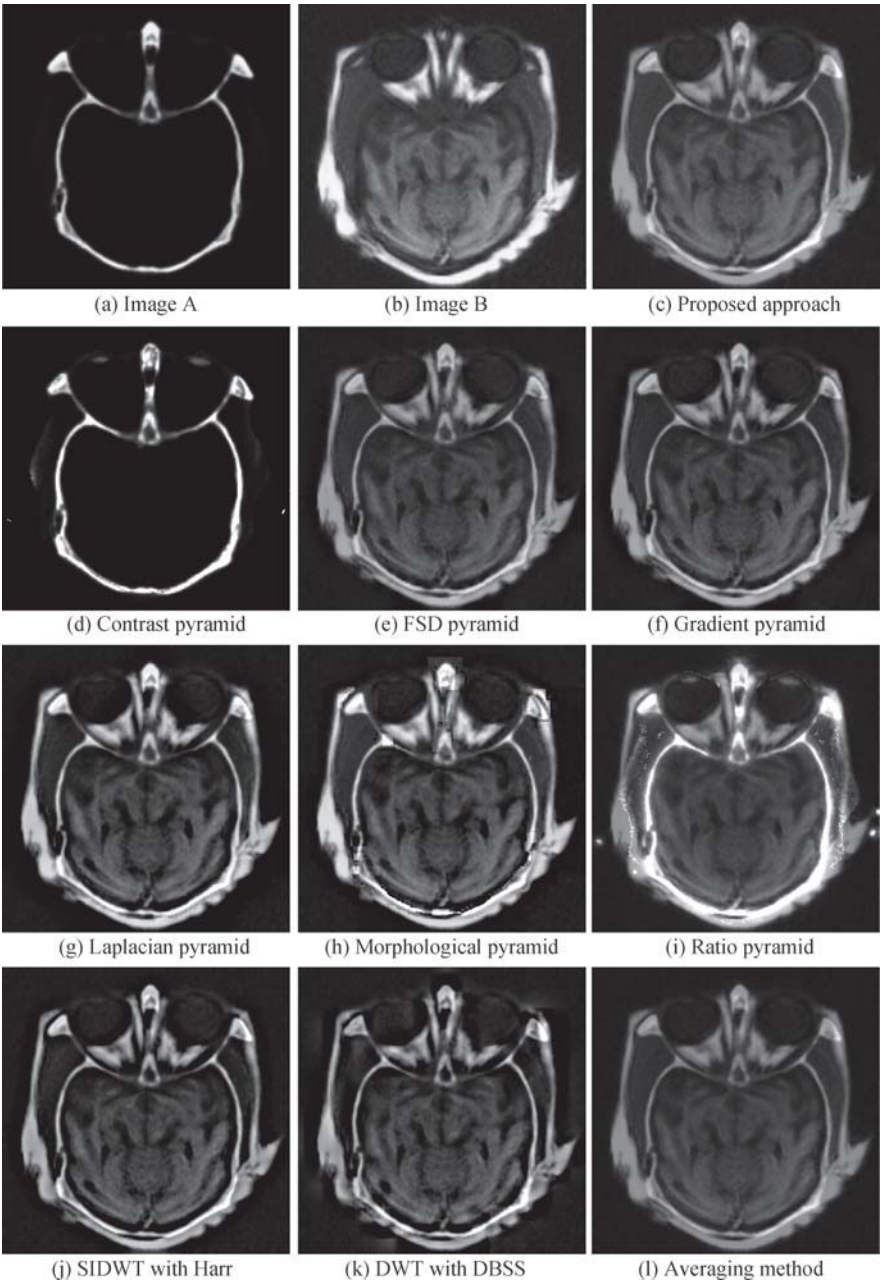

Fig. 6.3. Group 1 experimental images: (a) and (b) are original images; (c) – (l) are fused images

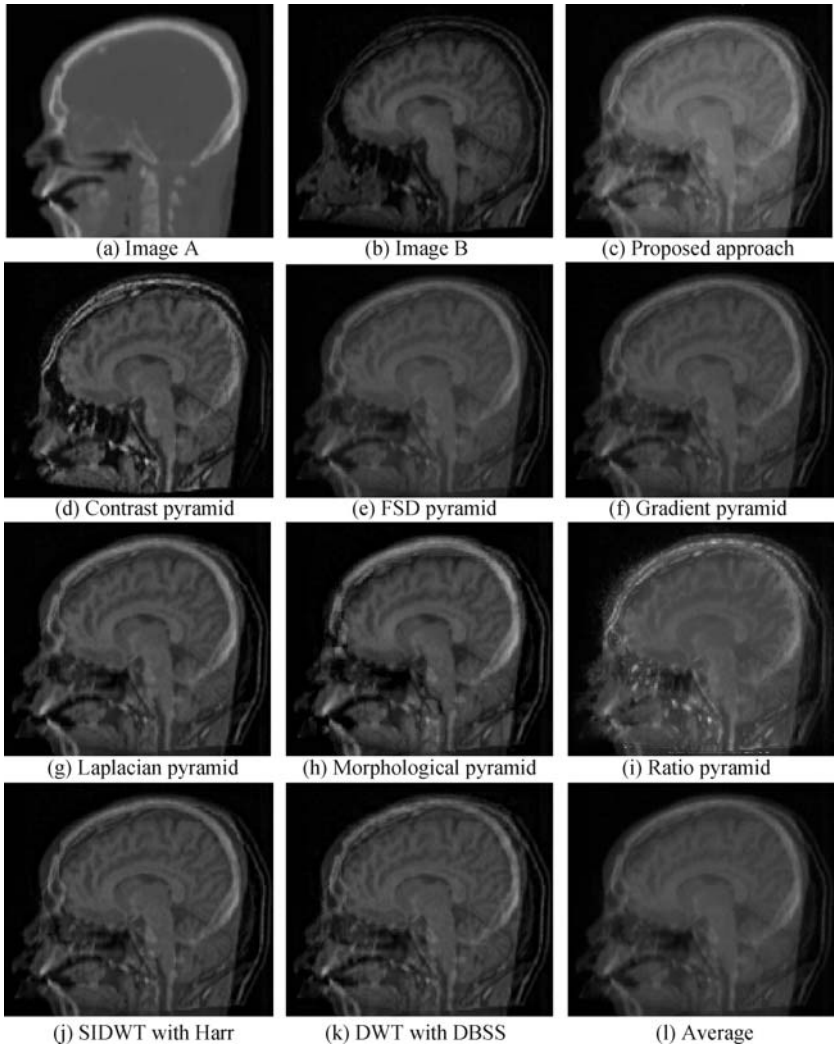

Fig. 6.4. Group 2 experimental images: (a) and (b) are original images; (c) – (l) are fused images

MI_AF and MI_BF; MI_AB shows the ability for a fused image to acquire information from image A and image B, so MI_AB is used here to evaluate different image fusion methods. A larger MI_AB indicates that the fused image acquires more information from image A and image B. In other words, the method with a largest MI_AB is superior to others among the various methods.

To show the better performance of the m-PCNN algorithm, several experiments are performed on four groups of 256-level images: Figs. 6.3(a) and (b) – Figs. 6.6(a) and (b). Each group consists of a pair of medical images from different sources. For example, images in Group 1 are acquired from the same position in the brain using different devices. Image A shown in Fig. 6.3(a) is a CT image that shows structures of bone, while Image B shown in Fig. 6.3(b) is an MR image that shows areas of soft tissues.

In clinical diagnosis or some research of pathology, doctors need to observe the position, the shape of both bone and tissue for judging disease or surveying organ's development. So the fused image is widely used in hospitals, which includes as much of the information in A and B as possible.

From Fig. 6.3, it is clearly observed that Fig. 6.3(d) does not contain the information in the image B; Fig. 6.3(i) contains false information that appears as bright spots, which does not exist in Image A or Image B; and Figs. 6.3(g) and (h) have a good contrast, however, investigating Fig. 6.3(h) carefully shows that there are also some sharp edges. Except for these four images, the remaining images look very similar. Three kinds of mutual information of group 1 are shown in Fig. 6.7 (Note, in Figs. 6.7 – 6.10, PA: Proposed approach; CP: Contrast pyramid; FSD: FSD pyramid; GP: Gradient pyramid; LP: Laplacian pyramid; MP: Morphological pyramid; RP: Ratio pyramid; SIDWT: SIDWT with Harr; DWT: DWT with DBSS; AM: Averaging method). Obviously, the proposed algorithm (PA) is superior to others because of its largest cumulative mutual information MI_AB. And the fused image acquires the most information from the image A and image B, then the better one comes to averaging method, the good one comes to morphological pyramid method and the worst one is the pyramid method.

In Group 2, Fig. 6.4(a) is a CT image and Fig. 6.4(b) is an MR image. Fused images are shown in Figs. 6.4(c) – (k). Ratio pyramid method is worse than the others because of so many bright spots in Fig. 6.4(i), which are false information. Also, Fig. 6.4(d) loses much information of edge in the mouth and Fig. 6.4(h) has bad edges. As shown in Fig. 6.8, IM_AB of the fused image with the m-PCNN algorithm is the biggest one, coming up the next is the averaging method, and morphological pyramid method lies in the third place. The last one is DWT with DBSS (2, 2) having the smallest mutual information.

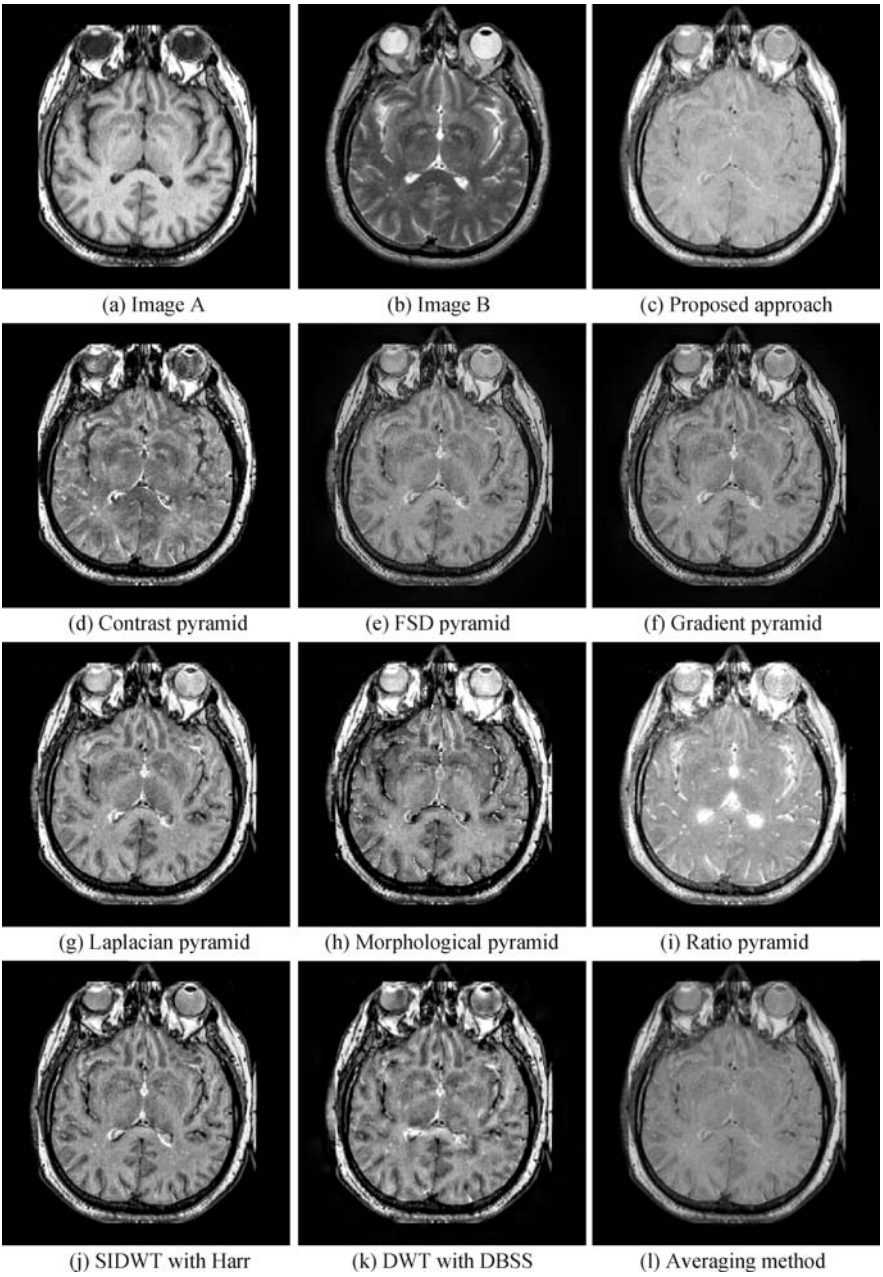

Fig. 6.5. Group 3 experimental images: (a) and (b) are original images; (c) – (l) are fused images

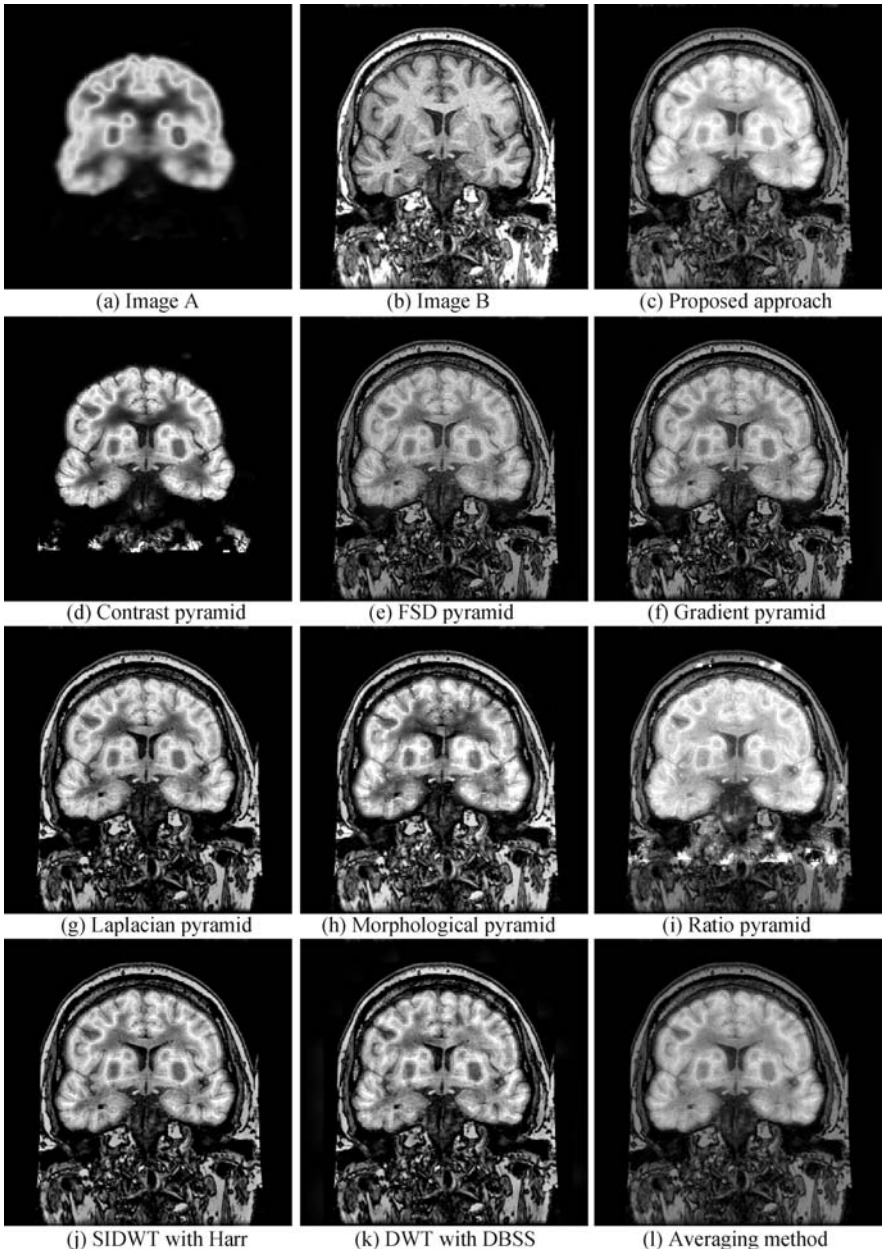

Fig. 6.6. Group 4 experimental images: (a) and (b) are original images, (c) – (l) are fused images

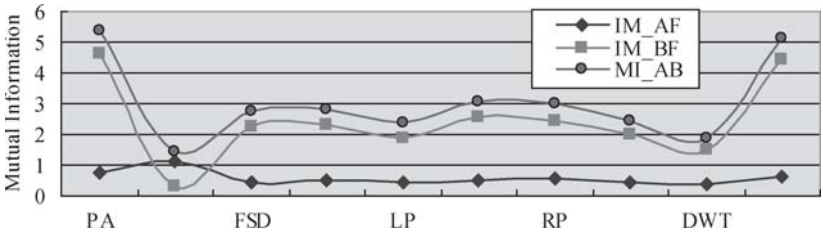

Fig. 6.7. Performance of different methods for Group 1

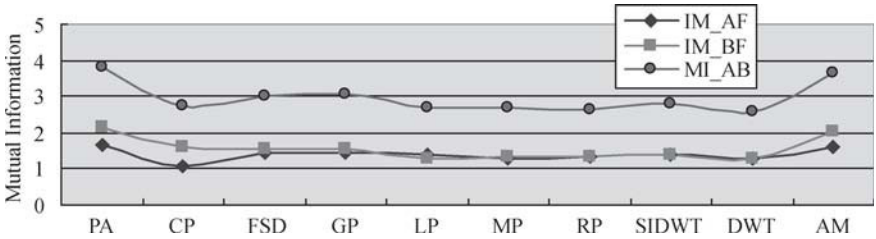

Fig. 6.8. Performance of different methods for Group 2

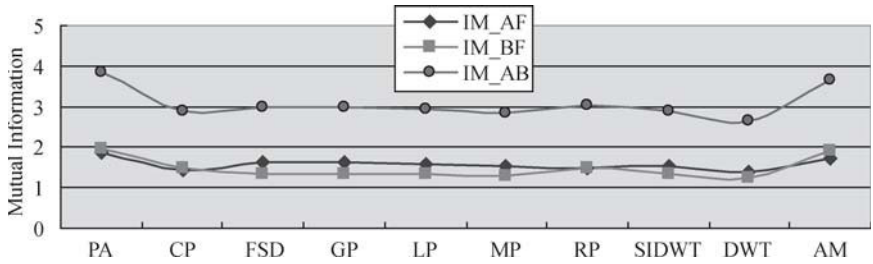

Fig. 6.9. Performance of different methods for Group 3

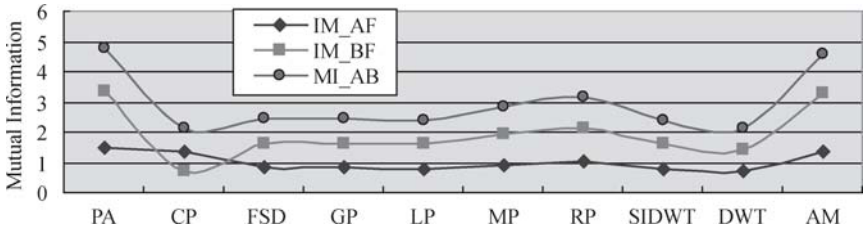

Fig. 6.10. Performance of different methods for Group 4

In Group 3 and Group 4, Fig. 6.5(a), (b) are transaxial brain images. The modality of Fig. 6.5(a) is MR-T1 and the modality of Fig. 6.5(b) is MR-T2. Fig. 6.6(a) is a coronal FDG image and Fig. 6.6(b) is a coronal MR-T1 image.

For Group 3 and Group 4, all the results are shown in Fig. 6.5 and Fig. 6.6. It has been observed clearly that some false edges appear in Fig. 6.5(h) and Fig. 6.6(h) fused with morphological pyramid, and most content of Fig. 6.6(b) is lost in Fig. 6.6(d) fused with contrast pyramid. Obviously, it is the worst result among these included methods.

As shown in Figs. 6.9 and 6.10, in all mutual information of these experiments for all included methods for Group 3 and Group 4, the IM_AB of image fused with the m-PCNN algorithm is the biggest, for these images contain the richest information from source images, and then comes to ratio pyramid method, whereas contrast pyramid method lies in the third place in Figs. 6.7 and 6.8.

According to the mutual information of all included methods, as shown in Figs. 6.7 and 6.10, the fusion performance of others varies depending on different images except the proposed m-PCNN algorithm and averaging method. That means both m-PCNN algorithm and the averaging ones are much more flexible and stable. Nevertheless, the proposed m-PCNN algorithm is always in the first place.

In summary, in the field of the medical image fusion, the proposed m-PCNN algorithm outperforms all other included methods. In addition, it has good flexibility and high stability.

6.3 Multi-focus Image Fusion

The multi-focus image fusion is the process to fuse several images of the same object obtained by different focus settings to produce a new image with extended depth of field, for the purpose of increasing the apparent depth of field. It plays an important role in many different fields such as biomedical imaging and computer vision. The multi-focus image fusion also is one of the main research branches in the field of the image fusion.

Generally, there are two common schemes for the multi-focus image fusion. The one is to use multi-resolution approaches, typically the discrete wavelet transform (DWT) and various pyramid algorithms [4 – 9]. But usually it is complicated and time-consuming and is difficult to implement. The other is based on the selection of image blocks from source images [18, 19]. The idea is to select the better resolution blocks corresponding to the same location

in source images to construct the fused image. Clearly, the latter is simpler than the former. However, the latter has some disadvantages. For instance, its fusion effect depends on the focus measurement to a great extent and usually there exist some errors (e.g., misjudgment or wrong selection of image blocks) in the fused image. Therefore, the multi-focus image fusion based on the PCNN was presented [2] and it will be discussed below.

Some multi-focus image fusion algorithms based on PCNN are presented in recent years. However, almost all methods employ more than one PCNN [13, 19] or combine the PCNN with other algorithms such as the DWT [16]. In order to make PCNN more suitable for the image fusion, the m-PCNN is designed and is applied to the multi-focus image fusion so that only one m-PCNN can finish the whole process of the multi-focus image fusion [2].

6.3.1 Dual-channel PCNN

The dual-channel neuron model, derived from the m-PCNN when $m = 2$, also consists of three parts: the dentritic trees, information fusion pool, and the pulse generator. The function of dentritic trees is to receive the stimulus including external inputs and surrounding neurons; information fusion pool is the place where all data are fused; the pulse generator is to generate the output pulse.

There are two input channels corresponding to two stimuli in the dual-channel neuron model. The model is described in the following Eqs. (6.3) – (6.7).

$$H_{ij}^{A}[n] = S_{ij}^{A} + \sum_{k,l} w_{ijkl} Y_{kl}[n-1]. \tag{6.3}$$

$$H_{ij}^{B}[n] = S_{ij}^{B} + \sum_{k,l} m_{ijkl} Y_{kl}[n-1]. \tag{6.4}$$

$$U_{ij}[n] = (1 + \beta_{ij}^{A} H_{ij}^{A}[n])(1 + \beta_{ij}^{B} H_{ij}^{B}[n]) + \sigma. \tag{6.5}$$

$$Y_{ij}[n] = \begin{cases} U_{ij}[n] - Sur_{ij}[n] & U_{ij}[n] > E_{ij}[n-1], \\ 0 & \text{Otherwise.} \end{cases} \tag{6.6}$$

$$E_{ij}[n] = \begin{cases} \mathrm{e}^{-\alpha_T} E_{ij}[n-1] & Y_{ij}[n] = 0, \\ V_T & \text{Otherwise.} \end{cases} \tag{6.7}$$

Compared with the basic PCNN, the dual-channel PCNN has a few parameters. In the dual-channel model, instead of the feed channel (F) and the link channel (L), H^A and H^B stand for two symmetrical input channels. β^A and β^B are the weighting coefficients of two symmetrical channels, σ is the level factor to adjust the average level of internal activity. Parameters ($U, E, Y, V_T, w_{ijkl}, m_{ijkl}$, and$\alpha_T$) have the same meanings as these in the basic PCNN model. Sur_{ij} denotes the input from surrounding neurons.

Generally,

$$k_{ijkl} = w_{ijkl} = m_{ijkl}, Sur_{ij} = \sum_{k,l} k_{ijkl} Y_{kl}[n-1].$$

Firstly, two channels of the neuron receive external stimuli and output of surrounding neurons. Furthermore, the data from these channels are weighted and mixed in the information fusion pool according to the weighting coefficients. Finally, the mixed data are released by the neuron as its output with the attenuation of the threshold. The implementation of the dual-channel PCNN is described as follows:

(1) Initialize parameters and matrices. $\boldsymbol{U} = \boldsymbol{O} = \boldsymbol{Y} = 0, \boldsymbol{E} = 1$.

The Initialization of $\boldsymbol{W}$ and $\boldsymbol{M}$ is different from that of other matrices. Here $\boldsymbol{K} = \boldsymbol{W} = \boldsymbol{M}$. Its values are determined empirically.

(2) If $\boldsymbol{S}^A = \boldsymbol{S}^B$, then $\boldsymbol{O} = \boldsymbol{S}^A$ or $\boldsymbol{S}^B$; and go to step (6).

(3) Normalize external stimuli's value in the range: [0, 1].

(4) $\boldsymbol{S}ur = \boldsymbol{Y} \otimes \boldsymbol{K}$;
$\boldsymbol{H}^A = \boldsymbol{S}^A + \boldsymbol{S}ur$;
$\boldsymbol{H}^B = \boldsymbol{S}^B + \boldsymbol{S}ur$;
$\boldsymbol{U} = (1 + \boldsymbol{\beta}^A * \boldsymbol{H}^A)(1 + \boldsymbol{\beta}^B * \boldsymbol{H}^B) + \sigma$.
If $\boldsymbol{U}_{ij} > \boldsymbol{E}_{ij}$ then $\boldsymbol{Y}_{ij} = \boldsymbol{U}_{ij} - \boldsymbol{Sur}_{ij}$, else $\boldsymbol{Y}_{ij} = 0$.
If $\boldsymbol{S}_{ij}^{\boldsymbol{A}} = \boldsymbol{S}_{ij}^{\boldsymbol{B}}$ or $\beta_{ij}^{\boldsymbol{A}} = \beta_{ij}^{\boldsymbol{B}}$, then $\boldsymbol{O}_{ij} = \boldsymbol{S}_{ij}^{\boldsymbol{A}}$ or $\boldsymbol{S}_{ij}^{\boldsymbol{B}}; else \boldsymbol{O}_{ij} = \boldsymbol{Y}_{ij}$.
If $\boldsymbol{Y}_{ij} = 0$ then $\boldsymbol{E}_{ij} = \exp(-\alpha_T) * \boldsymbol{E}_{ij}$, else $\boldsymbol{E}_{ij} = V_T$.

(5) If all neurons have been fired, go to (6), else go back to step (4).

(6) $\boldsymbol{O}$ is the output of the dual-channel PCNN.

The dual-channel PCNN model inherits essential features from the basic PCNN. For example, the dual-channel model remains the mechanism of synchronous pulse bursts, the exponential attenuation characteristic of the threshold. It is almost coincident with human visual characteristic. It is indispensable for the image processing.

Compared with the basic PCNN, the remarkable characteristic of the

dual-channel PCNN is that the number of external channels can easily be changed according to actual requirements, and this is also very useful when several images are fused at the same time.

6.3.2 Image Sharpness Measure

Image sharpness measure is very important for the multi-focus image fusion. Therefore, it is crucial to choose a good focus measure method to estimate image sharpness. In this subsection, some common evaluation methods of image sharpness will be described.

In Refs. [24, 25], the focus measure, the maximum for the best focused image, is defined and it generally decreases as the defocus increases. That is, the focus measure value of the focused image should be maximum, while that of the defocused one should be minimum.

Recently, there are many suggested focus measure methods, including variance, energy of the image gradient (EOG), energy of Laplacian of the image (EOL), and spatial frequency (SF). And they are described mathematically as follows:

Let $f(i,j)$ denote the gray level image with size of $M \times N$.

(1) Variance

$$\text{Variance} = \frac{1}{M \times N} \sum_i \sum_j [f(i,j) - \mu]^2, \tag{6.8}$$

where $$\mu = \frac{1}{M \times N} \sum_i \sum_j f(i,j).$$

This is the simplest way for the measure of the image fusion.

(2) Energy of image gradient (EOG)

$$\text{EOG} = \sum_i \sum_j (\mu_i^2 + \mu_j^2), \tag{6.9}$$

where, $\mu_i = f(i,j) - f(i+1,j); \mu_j = f(i,j) - f(i,j+1)$.

(3) Energy of Laplacian of the image (EOL)

$$\begin{aligned} EOL = \sum_i \sum_j [&-f(i-1,j-1) - 4f(i-1,j) - f(i-1,j+1) - \\ &4f(i,j-1) + 20f(i,j) - 4f(i,j+1) - f(i+1,j-1) - \\ &4f(i+1,j) - f(i+1,j+1)]^2. \end{aligned} \tag{6.10}$$

The high spatial frequencies associated with the image border sharpness are analyzed and measured by EOL which is implemented through Laplacian operator.

(4) Spatial frequency (SF)

$$SF = \sqrt{\frac{1}{M \times N}\sum_i \sum_j [f(i,j) - f(i+1,j)]^2 + \frac{1}{M \times N}\sum_i \sum_j [f(i,j) - f(i,j+1)]^2}. \tag{6.11}$$

Clearly, SF is a modified version of the energy of the image gradient (EOG).

Among these four measure methods, EOL method has the better performance, so it is used to measure image sharpness in the following subsection. Because evaluation of different focus measure methods is not our topic, more details can be found in Ref. [26].

6.3.3 Principle of Fusion Algorithm

The block diagram of dual-channel PCNN is shown in Fig. 6.11. Firstly, two parallel source images are directly inputted into these two channels. In the interior of this model each neuron can weigh the importance of both stimuli according to the clarity of input images. If both stimuli have obviously different sharpness or clarity, the sharper one should be better and selected. In this way, a sharper fused image will be obtained.

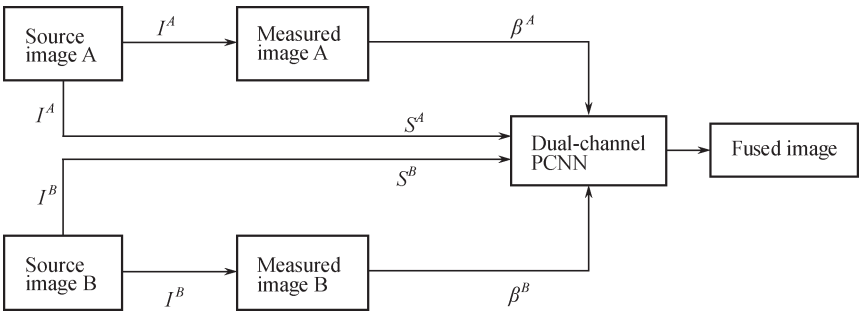

Fig. 6.11. Procedure of multi-image fusion

Therefore, the core of dual channel-PCNN is how to make sure that the weighting coefficients vary depending on the importance of input stimuli.

Here a new method is employed to implement the transformation from the importance of input stimuli to the weighting coefficients [27]. This method is explained in detail in the following paragraphs.

Let $A(i,j), B(i,j)$ denote the source images and $M_A(i,j)$ and $M_B(i,j)$ be the focus-measured images in Fig. 6.11. The difference between $M_A(i,j)$ and $M_B(i,j)$ is defined by $D(i,j) = M_A(i,j) - M_B(i,j)$. Generally speaking, if $D(i,j) > 0$, the pixel value at location (i,j) in image A should be chosen. Otherwise, its counterpart from image B will be chosen. However, in practice it is not sufficient to pick out the better focused image on a pixel-by-pixel basis only by this measure, since the result is vulnerable to wide fluctuations caused by outer environment such as various noises. So, it is necessary to maintain the robustness of the algorithm through more information from neighboring pixels.

In order to make full use of information contained in images, the value in a $(r+1) \times (r+1)$ region centered at $D(i,j)$ is summarized as $\bar{D}(i,j)$.

$$\bar{D}(i,j) = \sum_{m=-r/2}^{r/2} \sum_{n=-r/2}^{r/2} D(i+m, j+n). \tag{6.12}$$

Hence the weighting coefficients are

$$\beta_{ij}^{A} = \frac{1}{1 + e^{-\eta \bar{D}(i,j)}} \tag{6.13}$$

and

$$\beta_{ij}^{B} = \frac{1}{1 + e^{\eta \bar{D}(i,j)}}, \tag{6.14}$$

where η is a constant.

6.3.4 Implementation of Multi-focus Image Fusion

According to the above statements, the dual-channel PCNN used in the following experiments is a single layer two-dimensional array of laterally linked neurons and all neurons are identical. The number of neurons in the network is equal to that of pixels in the input image. In terms of position there exists a one-to-one correspondence between the image pixels ($I^A(i,j)$ and $I^B(i,j)$) and the neuron ($N(i,j)$). In other words, the external stimuli of $N(i,j)$ are $I^A(i,j)$ and $I^B(i,j)$.

As shown in Fig. 6.11, the implantation of the proposed multi-focus image fusion algorithm is described in the bellows, supposing that the input multi-focus images have been registered.

(1) Calculate the focus measure in Eq. (6.10) for two multi-focus images (I^A, I^B). And denote the measured images by M^A and M^B, respectively.

(2) Compute the weighting coefficients (β^A and β^B) via M^A and M^B.

(3) Input I^A and I^B as two stimuli into the dual-channel PCNN, and then start PCNN.

(4) Fuse the multi-focus images via the PCNN.

(5) Obtain the fused image after finishing the process of the PCNN.

6.3.5 Experimental Results and Analysis

This section consists of three parts: parameter setting, performance evaluation and practical applications.

The setting of parameters is very important to an algorithm. It affects the performance of the image fusion algorithm. But it is very difficult to choose the better parameters, hence, the dual-channel-PCNN's parameters are determined empirically. And its image fusion performance evaluation is carried out in succession by visual effect and objective evaluation criteria. At last, some of its applications are discussed.

Parameter setting

In the dual-channel PCNN, there are few parameters to be set. The weighting coefficients are determined by Eqs. (6.13) and (6.14). The other parameters settings are empirically shown in Table 6.2.

Table 6.2. Parameter setting in the experiment.

parameters	σ	α_T	V_T	r	η
value	–1	0.12	1000	14	0.01

Its convolution core

$$K = \begin{bmatrix} 1, & 0.5, & 1 \\ 0.5, & 0, & 0.5 \\ 1, & 0.5, & 1 \end{bmatrix}$$

and

$$M(\cdot) = W(\cdot) = Y[n-1] \otimes K$$

where $\otimes$ denotes convolution operation.

For comparison, besides the proposed method, several existing methods: principle component analysis (PCA), FSD pyramid, gradient pyramid (GP), morphological pyramid (MP), and SIDWT with Harr (SIDWT), are also employed. Their parameters are set as:

$$\text{pyramid level} = 4.$$

Selection rules:

$$\text{highpass} = \max,$$
$$\text{lowpass} = \text{average}.$$

Performance evaluation

To evaluate the performance of the proposed fusion method, extensive experiments on multi-focus images and different sensor images have been performed. Here, the experiments are divided into three groups. All images used in the experiment are shown in Fig. 6.12. From Group 1 to Group 3, images become more and more complicated for the purpose of testifying the performance of various algorithms in different environments.

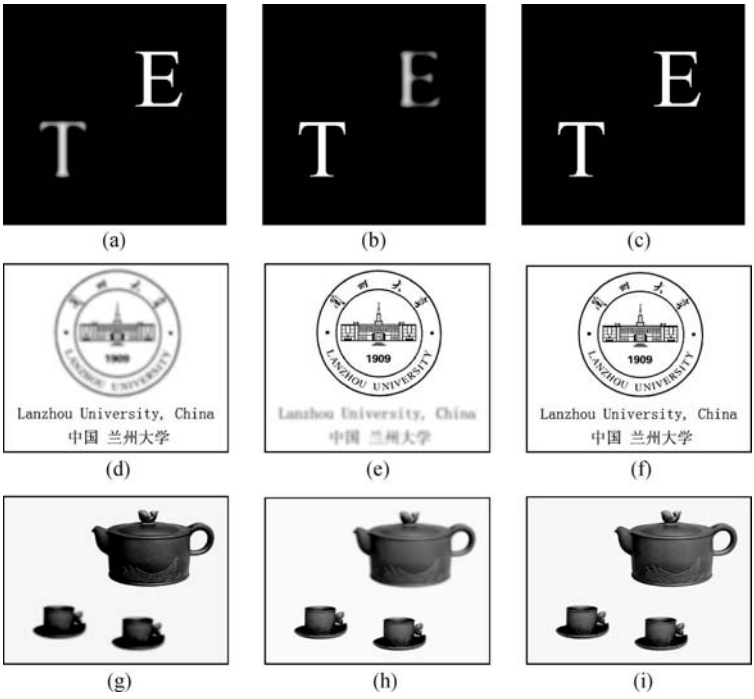

Fig. 6.12. Test images (Groups 1 – 3). (a) source image 1A; (b) source image 1B; (c) reference image 1R; (d) source image 2A; (e) source image 2B; (f) reference image 2R; (g) source image 3A; (h) source image 3B; (i) reference image 3R

Images in Figs. 6.13 – 6.15 are the experimental results obtained by the proposed methods and several comparison methods, and a reference image is also included in each group of figures. And then the performance of different algorithms is shown with objective standard in Fig. 6.16, respectively. Note that some abbreviations appear in these figures. Their meanings are: CP = contrast pyramid, FSD = FSD pyramid, GP = gradient pyramid, MP = morphological pyramid, SIDWT = SIDWT with Harr.

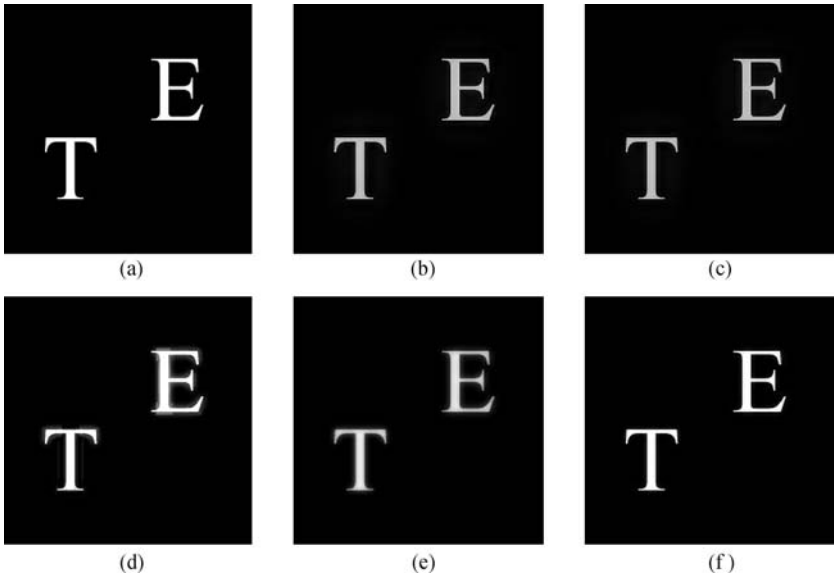

Fig. 6.13. Test results (Group 1). (a) Our method; (d) FSD method; (e) GP method; (f) MP method; (g) PCA method; (h) SIDWT method

For the evaluation of fusion performance, both subjective evaluation and objective evaluation should be taken into account. Subjective evaluation means assessing images just according to visual observation on them and determining which is the best. While objective evaluation means judging images by the value of a predefined function which may be in various forms.

For subjective evaluation, by observing Figs. 6.13 – 6.15 carefully it is clearly shown that the two images fused by FSD and GP methods have lower lightness and contrast than the others. MP method brings forth a good contrast but an unsatisfactory edge, as shown in Figs. 6.12(d), 6.13(d), and 6.14(d). PCA method is very poor in multi-focus image fusion, because its fused image (e.g., Figs. 6.12(f), 6.13(f), and 6.14(f)) is of neither high light-

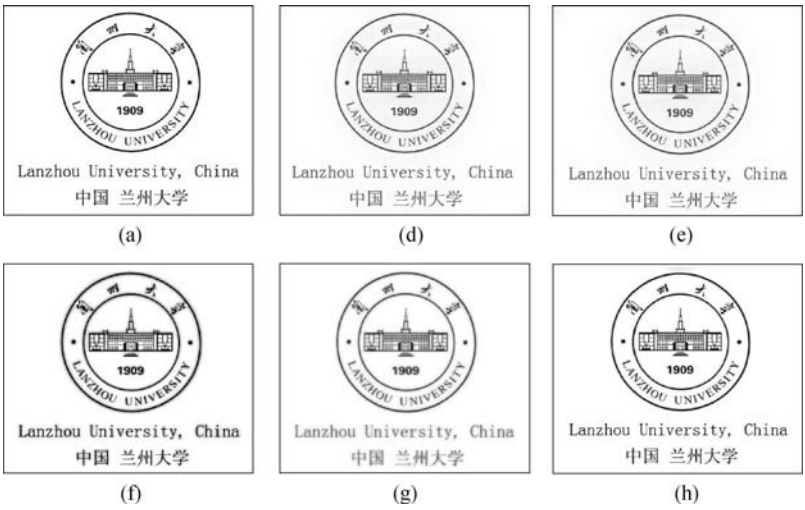

Fig. 6.14. Test results (Group 2): (a) Our method; (d) FSD method; (e) GP method; (f) MP method; (g) PCA method; (h) SIDWT method

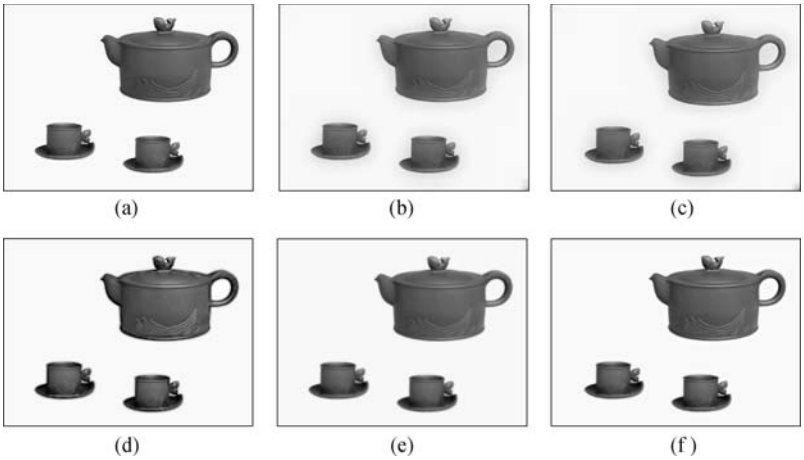

Fig. 6.15. Test results (Group 3) (a) Our method; (b) FSD method; (c) GP method; (d) MP method; (e) PCA method; (f) SIDWT method

ness nor fine detail. The rest four methods yield approximate visual effects. For objective evaluation, the root mean squared error (RMSE), defined as Eq. (6.15), is chosen as the evaluation criterion.

$$\mathrm{RMSE} = \sqrt{\frac{1}{M \times N} \sum_{i=1}^{M} \sum_{j=1}^{N} [F(i,j) - R(i,j)]^2}. \tag{6.15}$$

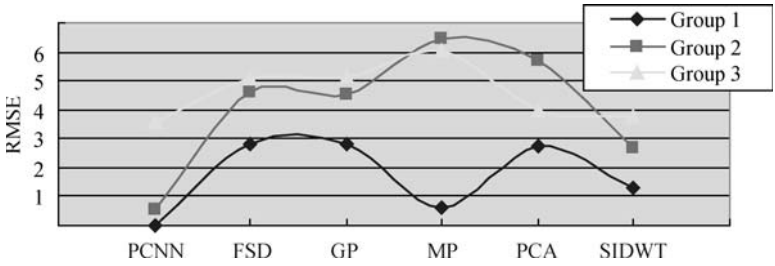

Fig. 6.16. Objective evaluation (PCNN denotes our proposed method)

In Eq. (6.15) R and F are a reference image and a fused image, respectively. Fig. 6.16 records all of RMSEs between the fused images and their reference ones.

In terms of objective evaluation, the proposed method is superior to others, seen from Fig. 6.16. For the RMSE, the smaller the value, the better the performance. In fact, the proposed method produces the smallest RMSE among the six algorithms. As a result, the method compared with the others is better in the multi-focus image fusion. In addition, because experimental images have different complexity, it also shows that the method is flexible for adaptability.

Practical applications

Two groups of microscope images shown in Fig. 6.17 are fused with dual

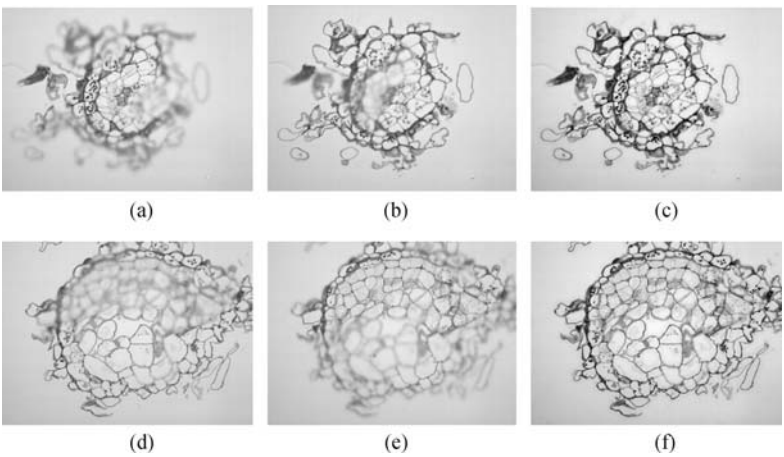

Fig. 6.17. Examples of microscope images: (a) image 1A; (b) image 1B; (c) image 1C; (d) image 2A; (e) image 2B; (f) image 2C

chnnel-PCNN algorithm. Image A and image B are source images with different focuses. Image C is the fused image. These fused images show that the proposed method is more practical and efficient. So, it can be widely applied in the field of multi-focus image fusion.

Summary

This chapter first recalls some preliminaries to image fusion. And then it introduces two methods of image fusion.

Because medical image fusion plays an important role in clinical applications, however, all methods previously proposed do not meet clinical demands completely. In this case the m-PCNN is introduced for the purpose of medical data fusion. Especially, the structure of PCNN is improved in a creative way, and several medical images are used to test the performance of the m-PCNN against other methods and experimental results show that the method is superior to any others.

Then, a multi-focus image fusion algorithm is introduced. Previous methods usually employ more than one PCNN models or a combination of PCNN with other methods such as DWT, while the proposed method just needs only one modified PCNN to implement multi-focus image fusion. Experimental results show that the presented method excels the existing methods in both visual effect and objective evaluation criteria. In practical applications, it has been proven that the method is more efficient.

In order to estimate the performance of various methods, the objective estimate standards are taken in the experiments. The experimental results show that the method outperforms the other methods compared and is efficient and very suitable for medical image fusion.

References

[1] Wang ZB, Ma YD (2008) Medical image fusion using m-PCNN. Information Fusion 9(2): 176 – 185

[2] Wang ZB, Ma YD, Gu J (2010) Multi-focus image fusion based on PCNN. Pattern Recognition 43(6): 2003 – 2016

[3] Wikipedia, the free encyclopedia. http: //en.wikipedia.org/wiki/Image_

fusion. Accessed 12 November 2007

[4] Anderson H (1987) A filter-subtract-decimate hierarchical pyramid signal analyzing and synthesizing technique. U.S. Patent, pp 718 – 104

[5] Burt PJ (1992) A gradient pyramid basis for pattern-selective image fusion. In: Proceedings of SID International Symposium: Society for Information Display, Playa del Rey, 1992, pp 467 – 470

[6] Burt PJ, Adelson EH (1983) The Laplacian pyramid as a compact image code. IEEE Transactions on Communications 31(4): 532 – 540

[7] Li H, Manjunath BS, Mitra SK (1995) Multisensor image fusion using the wavelet transform. Graphical Models and Image Processing 57(3): 235 – 245

[8] Rockinger O (1997) Image sequence fusion using a shift-invariant wavelet transform. In: IEEE International Conference on Image Processing, Santa Barbara, 26 – 29 October 1997

[9] Toet A (1989) A morphological pyramidal image decomposition. Pattern Recognition Letters 9(4): 255 – 261

[10] Toet A (1989) Image fusion by a ratio of low-pass pyramid. Pattern Recognition Letters, 9(4): 245 – 253

[11] Toet A, van Ruyven JJ, Valeton JM (1989) Merging thermal and visual images by a contrast pyramid. Optical Engineering 28: 789 – 792

[12] Kinser JM (1999) Spiral fusion using interchannel autowaves. In: Proceedings of SPIE, Stockholm, 22 – 28 June 1998

[13] Broussard RP, Rogers SK, Oxley ME et al (1999) Physiologically motivated image fusion for object detection using a pulse coupled neural network. IEEE Transactions on Neural Networks 10(3): 554 – 563

[14] Blasch EP (1999) Biological information fusion using a PCNN and belief filtering. In: IJCNN'99: Proceedings of International Joint Conference on Neural Networks, Washington, 10 – 16 July 1999

[15] Xu BC, Chen Z (2004) A multisensor image fusion algorithm based on PCNN. In: WCICA 2004: the 5th World Congress on Intelligent Control and Automation, Hangzhou, 15 – 19 June 2004

[16] Wei L, Zhu XF (2005) A New Image Fusion algorithm based on wavelet packet analysis and PCNN. In: ICMLC '05: the 4th International Conference on Machine Learning and Cybernetics, Guangzhou, 18 – 21 August 2005

[17] Zhang JY, Liang JL (2004) Image fusion based on pulse-coupled neural networks. Computer Simulation 21(4): 102 – 104

[18] Li M, Cai W, Tan Z (2006) A region-based multi-sensor image fusion scheme using pulse-coupled neural network. Pattern Recognition Letters 27(16): 1948 – 1956

[19] Miao Q, Wang B (2005) A novel adaptive multi-focus image fusion algorithm based on PCNN and sharpness. In: Proceedings of SPIE, Orlando, 28 March-1 April 2005

[20] Wei H, Jing ZL (2007) Multi-focus image fusion using pulse coupled neural network. Pattern Recognition Letters 28(9): 1123 – 1132

[21] The Online Resource for Research in Image Fusion. http: //www.imagefusion.org. Accessed 20 Oct 2007

[22] Shen Y, Ma JC, Ma LY (2006) An adaptive pixel-weighted image fusion algorithm based on local priority for CT and MRI images. In: the IEEE Instrumentation and Measurement Technology Conference, Sorrento, 24 – 27 April 2006

[23] AtIas.http: //www.med.harvard.edu/AANLIB/home.html. Accessed 20 Oct 2007

[24] Krotkov E (1988) Focusing. International Journal of Computer Vision 1(3): 223 – 237

[25] Ligthart G, Groen F (1982) A comparison of different autofocus algorithms. In: IEEE the 6th International Conference on Pattern Recognition, Munich, 1982

[26] Wei H, Jing ZL (2007) Evaluation of focus measures in multi-focus image fusion. Pattern Recognition Letters 28(4): 493 – 500

[27] Eltoukhy HA, Kavusi S (2003) A computationally efficient algorithm for multi-focus image reconstruction. In: Proceedings of SPIE Electronic Imaging, San Jose, 20 January 2003